# Rational Catalyst Structural Design to Facilitate Reversible Li-$CO_2$ Batteries with Boosted $CO_2$ Conversion Kinetics

Shiming Chen[1†], Kai Yang[2†*], Hengyao Zhu[1], Jianan Wang[3], Yi Gong[2], Huanxin Li[4], Manman Wang[2], Wenguang Zhao[1], Yuchen Ji[1], Feng Pan[1], S. Ravi P. Silva[2], Yunlong Zhao[5,6*], Luyi Yang[1,*]

[1] School of Advanced Materials, Peking University, Shenzhen Graduate School, Shenzhen 518055, China

[2] Advanced Technology Institute, University of Surrey, Guildford, Surrey, GU2 7XH, UK

[3] Department of Environmental Science and Engineering, State Key Laboratory of Multiphase Flow in Power Engineering, Xi'an Jiaotong University, 28 Xianning West Road, Xi'an 710049, China

[4] Department of Engineering, University of Cambridge, 9 JJ Thomson Avenue, Cambridge, CB3 0FA, UK

[5] Dyson School of Design Engineering, Imperial College London, London, SW7 2BX, UK

[6] National Physical Laboratory, Teddington, Middlesex, TW11 0LW, UK

[†] These authors contributed equally to this work.

*Correspondance: kai.yang@surrey.ac.uk; yunlong.zhao@imperial.ac.uk; yangly@pkusz.edu.cn

## Abstract

Lithium-$CO_2$ batteries (LCBs) are regarded as a promising energy system for $CO_2$ drawdown and energy storage capability which has attracted widespread interest in carbon neutrality and sustainable societal development. However, their practical application has been limited by slow kinetics in catalytic reactions and poor reversibility of $Li_2CO_3$ products which leads to the issue of a large overpotential, low energy efficiency and poor reversibility. Herein, an efficient catalyst design and synthesis strategy is proposed to overcome the abovementioned bottleneck. Through an electrical joule heating procedure, Pt with random crystal orientations is converted into a 3D porous Pt catalyst with preferred (111) crystal orientation within seconds, exhibiting enhanced $CO_2$ conversion kinetics with superior electrochemical performance. This includes ultralow overpotential (0.45 V), fast rate charging (up to 160 μA $cm^{-2}$) and high stability (over 200 cycles under 40 μA $cm^{-2}$). A proof-of-concept stacked Li-$CO_2$ pouch cell, with stable operation under practical current density is demonstrated, indicating significant potential for large-scale operations. This bottom-up design of efficient catalysts and synthesis strategy offers a rapid and cost-effective approach to maximizing catalytic sites for $CO_2$ conversion under restricted catalyst loading, showcasing its versatility across a broad spectrum of catalyst-based energy conversion and storage systems.

**Keywords:** Li-$CO_2$ battery, $CO_2$ conversion, Joule heating, Electrocatalyst, Pouch cell

## Introduction

The massive consumption of non-renewable fossil fuels has caused increasingly energy shortage issues and corresponding $CO_2$ emissions also trigger serious environmental crises such as global warming and extreme climate change.[1, 2] New negative emissions technologies to both address the ever-increasing energy demand and reduce $CO_2$ emissions are of great importance for carbon neutrality and the sustainable development of human society.[3, 4] Among the novel carbon dioxide capture and utilization technologies (e.g., $CO_2$ reduction techniques),[5-7] metal-$CO_2$ batteries have attracted considerable attention due to their unique characteristic of $CO_2$ recyclability and providing green energy storage simultaneously.[8, 9] With $CO_2$ as the reactant, rechargeable Li-$CO_2$ batteries (LCBs) deliver a high theoretic energy density of 1876 Wh $kg^{-1}$ and theoretical equilibrium potential at ~2.8 V (vs. $Li/Li^+$, based on the reaction of $3CO_2+4Li \leftrightarrow 2Li_2CO_3+C$ ), which is substantially higher than that of high-energy lithium-ion battery systems (e.g., ~300 Wh/kg of Si-graphite//NCM systems). The direct utilization of CO2 in energy conversion and storage devices also provide effective approaches for the sustainable development of carbon neutral society. These advantages make LCBs as promising next-generation energy storage devices not only for substitution of conventional Li-ion batteries but also extended application in aerospace exploration (especially on predominant $CO_2$ environments, such as Mars).[10]

Despite being very promising and extensively investigated since its emergence, the widespread applications of LCBs still suffer from several thorny research bottlenecks. The sluggish $CO_2$ conversion leads to large overpotential (> 1 V), low energy efficiency (< 75%) and inferior rate performance (normally operated at 0.1 C).[10, 11] The poor reversibility caused by the incomplete decomposition of insulating $Li_2CO_3$ products and the unexpected side reactions (e.g. electrolyte decomposition, carbon corrosion, etc. at high charging potentials) leads to limited cycle life.[12, 13] The lack of rational electrode and electrocatalyst structure design fails to ensure large-scale practical application and exhibits uncompetitive areal capacity (< 1 mAh $cm^{-2}$).[14] Therefore, the key challenge to promote LCBs performance lies in the development of highly efficient cathode electrocatalysts. To this end, tremendous efforts have been devoted to investigating various electrocatalysts such as carbon-based materials (graphene, carbon nanotubes, carbon aerogel, porous activated carbon, etc.), transition metal compounds (oxide, sulphide, carbide, etc.), and noble metal/alloys (Pt, Ir, Ru, etc.).[8, 10, 12] Despite efforts to improve electrochemical performance, many electrocatalysts have not yet demonstrated satisfactory results when evaluated under practical operating conditions such as higher operating current density and larger electrode size.

On the other hand, achieving a balance between long-term durability, high catalytic performance,

and cost control remains a challenge.[10, 12] For instance, the development of single-atom electrocatalysts has been pursued to reduce costs, but some have exhibited susceptibility to side reaction chemicals (e.g., carbon monoxide) during $CO_2$ conversion, leading to structural damage and limited cycle life.[15-21] Additionally, incomplete exposure of catalytic sites for $CO_2$ conversion can result in suboptimal rate performance.[16, 22] Thus, designing catalysts with an optimal crystal structure to maximize catalytic sites for $CO_2$ conversion is a critical principle to consider.

Herein, we demonstrate an efficient modulation strategy of the catalyst structure to enhance $CO_2$ conversion kinetics and improve the overall electrochemical performance of LCBs. Following the theoretic simulations on the preferred Pt facet for LCBs reactions, electrical Joule heating is employed to regulate both the structural and morphological properties of Pt-based electrocatalysts which are expected to enhance the $CO_2$ conversion reaction and increase catalytic reaction sites respectively. This bottom-up design of efficient catalysts synthesis strategy offers a rapid, cost-effective, and controllable approach to maximizing catalytic sites for $CO_2$ conversion under restricted catalyst loading. Also, this strategy showcases versatility across a broad spectrum of catalyst-based energy conversion and storage systems. With restricted areal mass loading of Pt catalyst, the as-developed porous electrocatalyst exhibits superior electrochemical performance over currently reported studies including low overpotential (< 0.5 V), excellent rate performance (up to 1.6 C, 1 C = 100 μA $cm^{-2}$), and high stability under elevated current density (over 200 cycles under 0.4 C). Moreover, stacked Li-$CO_2$ pouch cells can be fabricated and operated under more practical operation conditions (280 $mAh_{cell}$, and cycled at 0.2 C with over-potential < 0.6 V).

**Structural regulation and engineering for Pt catalyst**

According to previous studies, the reaction process in platinum-based LCBs can be described with the following reversible equations: $3CO_2+4Li \leftrightarrow 2Li_2CO_3+C$ (**Figure 1a**). DFT calculations were first conducted to compare the electrocatalytic $CO_2$ reduction reaction ($CO_2RR$) and $CO_2$ evolution reaction ($CO_2ER$) activity on different orientations of Pt. In the typical $CO_2RR$ process, the most important parameters to evaluate the LCBs performance are the adsorption of the reactant ($CO_2$ and lithium ions) and the reaction product ($Li_2CO_3$ and C). The $CO_2$ conversion kinetics is mainly dominated by catalysts in LCBs, as the supporting carbon matrix (e.g., carbon paper, carbon cloth.) generally exhibits poor catalytic performance toward $CO_2$ conversion.[23] The adsorption energy of $CO_2$, $Li^+$ and $Li_2CO_3$ on typical thermodynamically stable surfaces (i.e. (111), (200) and (220)) of Pt are calculated (adsorption configuration in **Figure 1b**). For the $CO_2$ reactant, Pt (111) facet exhibits the largest adsorption energies (-0.43 eV) compared with (200) and (220) facets as shown in **Figure 1c**. Meanwhile, the adsorption energy for $Li^+$ on Pt (111) facet (-1.12 eV) is much higher than that of

the other two facets, which indicates the higher lithiophilicity on the Pt (111) facet. Thus, from the reactant perspective, Pt (111) exhibits the best compatibility and adsorption toward $CO_2$ and $Li^+$, indicating a larger concentration of reactants on the catalyst surface to promote higher $CO_2$RR activity.[24] The adsorption behaviour of the main reaction product ($Li_2CO_3$) is further calculated, Pt (111) exhibits larger adsorption energy of -1.53 eV than (200) and (220) facets. In this case, $Li_2CO_3$ can be more easily generated on Pt (111), leading to an enhanced reaction activity for potentially higher rate and capacity performance.[25]

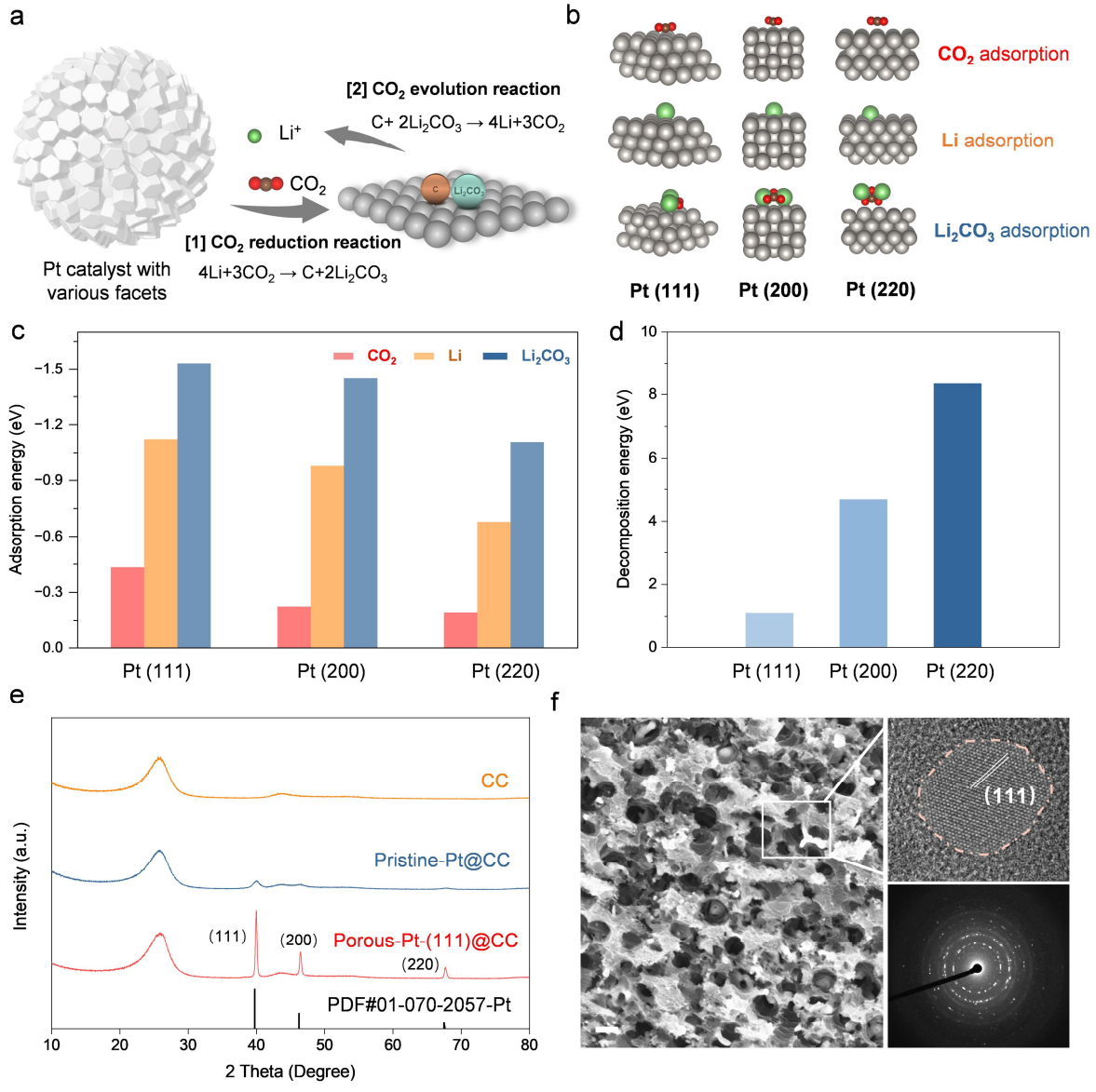


**Figure 1. Design and characterizations of Pt electrocatalyst.** (a) Schematic $CO_2$ conversion process in Pt-based LCBs. (b) Side view of adsorption behaviour of $CO_2$, Li and $Li_2CO_3$ on different orientations of Pt surface and (c) comparison of corresponding adsorption energy. (d) Decomposition energy of $Li_2CO_3$ on different orientations of Pt surface. (e) XRD analysis of different electrodes. (f) Detailed surface structure and TEM observation of the electrode after HTS (scale bar = 200 nm).

The sluggish decomposition of $Li_2CO_3$ has been considered the rate-determining step for the $CO_2ER$ process in LCBs. The large overpotential for the decomposition of $Li_2CO_3$ during $CO_2ER$ greatly reduces the energy efficiency and further results in limited cycle life owing to the incomplete decomposition of discharging product and electrolyte instability under high charging potential.[16, 22] A low decomposition energy barrier of $Li_2CO_3$ could promote its complete decomposition, thus improve the cycling stability of the battery. The decomposition barrier of $Li_2CO_3$ ($C + Li_2CO_3 \rightarrow Li^+ + LiC_2O_3 + e^-$) is evaluated as shown in **Figure 1d**. As a result, Pt (111) also exhibits the lowest decomposition energy of $Li_2CO_3$ (1.09 eV) among the three typical facets, hence in favour of $Li_2CO_3$ dissociation. According to the above theoretical calculations, Pt (111) has been identified as the most active interfacial facet to catalyse both $CO_2RR$ and $CO_2ER$ for LCBs.

High-temperature shock (HTS), as a non-equilibrium extreme method based on the electrical Joule heating, has been regarded as a low cost and highly efficient technique to regulate morphology and structure properties of diverse functional nanomaterials.[26, 27] Next, we employed HTS technique to regulate the crystal orientation and exposed active sites on Pt catalysts (**Figure S1**). Carbon cloth (**Figure S2**) with good conductivity, flexibility and porosity was used as the electrode substrate.[23, 28] Firstly, Pt was uniformly deposited on the carbon cloth (CC) via thermal evaporation (**Figure S3**), and the resulting areal mass loading of Pt is ~ 0.1 mg $cm^{-2}$. The Pt-coated carbon cloth (pristine-Pt@CC) was further loaded on the HTS holder (**Figure S4**) and thermal-treated under vacuum conditions with a cut-off heating temperature of 1500 °C (**Figure S5**).

After 2 seconds of HTS process, the loaded Pt melted during the rapid temperature rise, and then self-assembled into nanoparticles during the abrupt temperature drop.[29] Transmission electron microscopy (TEM) observation identified the existence of nanoparticles with a size range of 5-10 nm (**Figure S6**). The structural information of different air electrodes was investigated by X-ray diffraction (XRD) as shown in **Figure 1e**. The broad peak at around 26° in all three electrodes can be ascribed to the carbon fibre of the CC substrate. After the Pt deposition, weak Pt peaks at (39.9°) can be identified according to the standard PDF cards (01-070-20057).[30] In sharp contrast, the (111) peak was greatly intensified after the HTS treatment, indicating the successful implementation of the preferred orientation of Pt (111) which was demonstrated by TEM.[31, 32] Besides, XRD patterns with fitting data (**Figure S7**) showed a significantly increased content of (111) facet from 48.6 % to 63.6 % and the narrowed full width high maximum values also suggested larger crystalline grains. The lattice spacing of 0.225 nm can be observed, corresponding to the (111) crystal plane of Pt, which is also confirmed by the speckle rings of the selected area electron diffraction pattern (**Figure 1f**).[33, 34] With more observation of other nanoparticles, it was found that the Pt (111) orientations dominated the surface of nanoparticle platinum (**Figure S8**). To elucidate theAs origin of preferred

Pt (111) orientation during HTS process, surface energies of (111), (200) and (220) facets of Pt are compared in **Figure S9**. Pt (111) facet exhibited the lowest surface energy (1.44 J $m^{-2}$) compared with (200) and (220) facets, which indicates that the (111) facet is a more thermodynamically stable facet. Thus, Pt (111) orientation exposed more during the abrupt cooling process.[35] Such approach could be adopted to synthesizing other metallic catalysts with desirable crystalline orientations.

Moreover, the dense thin-film morphology of the pristine Pt-coated electrode was transformed into a 3D porous structure (**Figure S10** and **Figure S11**). The $N_2$ adsorption-desorption isotherm of the HTS-treated catalyst (**Figure S12**) shows a typical hysteresis loop characteristic of a porous structure.[36] The introduced porosity not only significantly increased the specific surface area from 0.66 $m^2$ $g^{-1}$ to 1.25 $m^2$ $g^{-1}$ but also created hierarchical pore size distribution on the electrode surface.[37] Finite element method analysis was then employed to simulate the $CO_2$ flow on the surface of different electrodes (see **Figure S13** and **Figure S14** for detailed results). As a result, catalyst with porous structure allows faster $CO_2$ diffusion. In addition, such 3D porous catalyst structure is expected to promote electrolyte permeation and increase catalytic sites to facilitate $CO_2$ conversion.

## Enhanced $CO_2$ conversion kinetics and reversibility

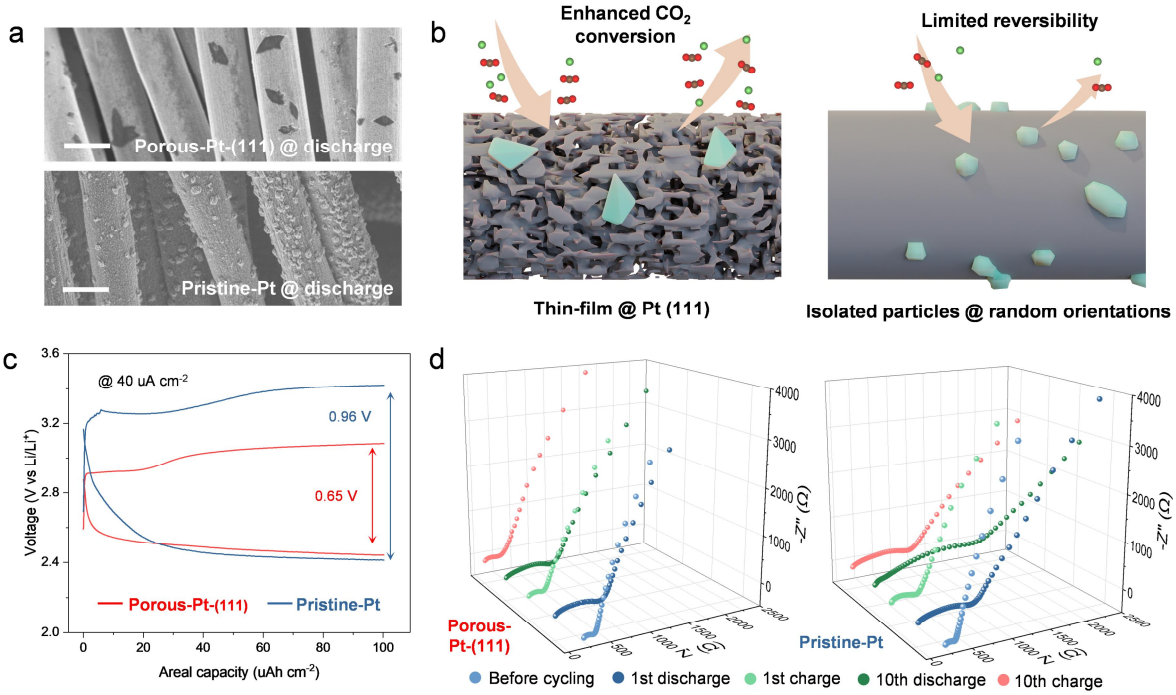


**Figure 2. Enhanced $CO_2$ conversion and reversibility for Li-$CO_2$ battery.** (a) Electrode morphology at discharging state (scale bar = 10 μm). (b) Schematic illustration of the different $CO_2$ conversion processes on the catalysts. (c) Galvanostatic charge/discharge curves under the current density of 40 μA $cm^{-2}$. (d) EIS spectra during cycling.

After the Pt (111) preferred orientations and porous catalyst structure were successfully introduced

in the air electrode, the $CO_2$ conversion process was then evaluated in Li-$CO_2$ batteries under $CO_2$ atmosphere (**Figure S15**). The maximum areal capacity was first measured with a cut-off voltage at 2 V and under a current density of 20 μA $cm^{-2}$ (**Figure S16**). Notably, the porous-Pt-(111)@CC enabled a high areal capacity of 5.8 mAh $cm^{-2}$, which is more than twice the capacity delivered by pristine-Pt@CC (2.6 mAh $cm^{-2}$). To evaluate the utilization efficiency of Pt, the normalized specific areal capacity (areal capacity divided by the areal mass loading of Pt) is defined and compared with the reported literature as shown in **Figure S17**. The porous-Pt-(111)@CC delivered the highest normalized specific areal capacity (58.1 Ah $g^{-1}_{catalyst}$) with the minimum catalyst loading among all the listed catalysts (**Table S2**), suggesting a highly efficient utilization of the catalyst to promote $CO_2$ conversion. Besides, the discharging voltage of porous-Pt-(111)@CC also outperforms pristine-Pt@CC under the same operating condition. The significantly improved areal capacity is contributed by the elevated specific surface and porous catalyst morphology that provide more available sites to accommodate the reaction product; meanwhile, higher contents of exposed preferred Pt (111) orientation accelerate $CO_2$ conversion and product generation during the $CO_2$RR process. Interestingly, distinctively different morphologies for the discharging product could be observed on porous-Pt-(111)@CC and pristine-Pt@CC (**Figure 2a** and **Figure S18**). For pristine-Pt@CC, the discharging products tend to form isolated micro-sized particles following the Volmer-Weber mode due to the lack of catalytic sites, leading to residual $CO_2$RR products on the electrode surface (**Figure S19**). As illustrated in **Figure 2b**, Benefiting from abundant and highly efficient catalytic sites, thin-film products are formed on porous-Pt-(111)@CC following the Frank-van der Merwe mode which can easily decompose upon the charging process (**Figure S20**).[38]

The cyclic voltammetry (CV) tests (**Figure S21**) of the Li-$CO_2$ batteries were conducted at the scan rate of 1 mV $s^{-1}$ within the potential range from 2.0 to 3.5 V to observe the redox reaction process for different electrocatalysts. The cathodic peaks started at 2.5 V corresponding to the $Li_2CO_3$ and carbon formation during the $CO_2$RR process. And during the anodic scanning, the peaks started at 2.8 V can be ascribed to the decomposition of the discharging product. The porous Pt catalyst showed a larger reaction current and lower overpotential during charging compared with the pristine Pt catalyst and pure carbon electrode (CC) (**Figure S22**), indicating an enhanced $CO_2$ utilization during $CO_2$RR and facilitated decomposition of reaction product during $CO_2$ER. Galvanostatic charging and discharging tests were carried out as shown in **Figure 2c**. To make a better comparation with recent LCB literature, the cut-off capacity was accordingly set as 100 μAh $cm^{-2}$. Considering the practical application of LCBs, a moderate operating current density of 40 μA $cm^{-2}$ was applied. Porous-Pt-(111)@CC exhibits a charging plateau of 3.08 V with an overpotential of merely 0.65 V, which is one of the lowest values among all reported electrocatalysts (excluding

the photo-electrocatalyst or redox mediator works) in LCBs under the same current density.

Since the reaction kinetics of $CO_2RR$ and $CO_2ER$ have a great impact on reversibility, electrochemical impedance spectra (EIS) were recorded during cycling to evaluate the overall reversibility of LCBs. The generation of reaction product during discharging will passivate the electrode, hence increasing the interfacial charge transfer resistance ($R_{ct}$) for both catalysts (**Figure 2d** and **Table S1**). Upon the charging process of the first cycle, the resistance recovered nearly to the pristine state before cycling for porous-Pt-(111)@CC, confirming the complete decomposition of the discharging product. By contrast, $R_{ct}$ for pristine-Pt@CC was partially recovered at the charged state, indicating residual discharging product on the electrode. $R_{ct}$ for pristine-Pt@CC became even higher after 10 cycles, suggesting a deteriorating interface, whereas porous-Pt-(111)@CC exhibited well-maintained interfacial resistance owing to the high reversibility.

To obtain the correlation between the componential information on electrode surfaces and the cell reversibility, LCBs under different states of charge were disassembled for ex-situ interfacial spectroscopy analysis. The ex-situ XPS (**Figure S23** and **Figure 3a**) analysis of both catalysts exhibit distinctive $Li_2CO_3$ signals in both C 1s (290.3 eV) and Li 1s spectra (55.5 eV) at discharged state, confirming the generation of $Li_2CO_3$.[36, 39] In the following charging process, all signals belonging to $Li_2CO_3$ disappeared on porous-Pt-(111)@CC, suggesting the complete decomposition of $Li_2CO_3$. However, partial $Li_2CO_3$ could still be detected on pristine-Pt@CC at charged state. Ex-situ Raman (**Figure 3b**) and FTIR (**Figure S24**) were also employed to reveal the reversibility of the catalyst-dependent $CO_2$ conversion. Consistent with the XPS measurement, porous-Pt-(111)@CC enhanced the reversible decomposition of discharging product $Li_2CO_3$ as confirmed by the evolution of typical Raman stretching peaks (~1090 $cm^{-1}$) and FTIR spectra (~1510 $cm^{-1}$).[40-43] Besides, XRD measurements for different electrochemistry states were analysed (**Figure S25**). It could be observed that the characteristic peak (21.34°, 30.64° and 31.79°) of $Li_2CO_3$ disappeared in the charging state on porous-Pt-(111)@CC.[10]

It is reported that the nanostructure of the catalyst can affect the growth/evolution of discharging product on the catalyst surface.[36, 38] In return, the repeated catalytic behaviour will also introduce reaction stress and change the catalyst structure.[44, 45] The accumulation of incompletely decomposed discharge product will passivate the catalyst surface and worse still lead to catalyst structural collapse or detachment from the substrate owing to the residue stress.[44, 46] The disassembled air electrodes were also observed by scanning electron microscope (SEM) (**Figure 3c**). Surprisingly, the air electrode with pristine Pt catalyst suffered severe structure destruction. The pristine Pt catalyst was peeled off the carbon fibre and the non-active carbon substrate was exposed. While in the air electrodes with porous Pt catalyst, the structural integrity was maintained stable

during cycling with the porous Pt catalyst structure well preserved. Based on the above results, it can be concluded that porous-Pt-(111)@CC facilitates the complete decomposition of thin film discharging product during charging owing to abundant and highly efficient catalytic sites, hence improve the excellent electrochemical reversibility. The porous structure is also beneficial to the dissipation of the reaction stress to maintain electrode structure integrity (**Figure 3c**); while the residual $Li_2CO_3$ on pristine-Pt@CC gradually accumulates, and eventually causes structure disintegration of the electrode owing to Pt detachment from the substrate. Furthermore, the SEM results of porous-Pt-(111)@CC after long-term cycling also confirmed the improved reversibility of $Li_2CO_3$ decomposition (**Figure S26**).

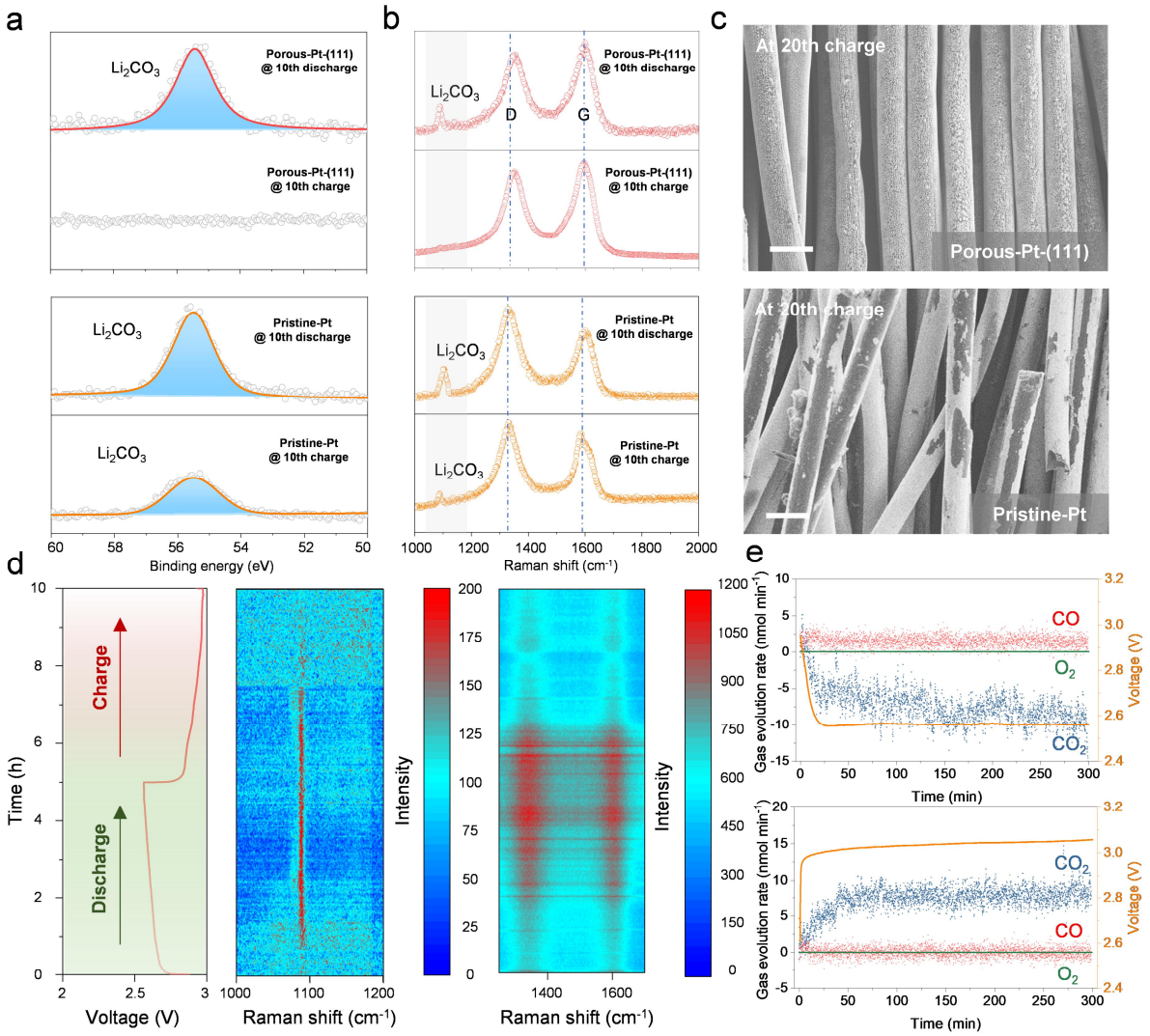


**Figure 3. Characterizations of the reversibility.** (a) Li 1s XPS spectra for air electrodes under different electrochemical status: discharge state and charge state. (b) Ex-situ Raman analysis of the cycled air electrodes. (c) SEM images of different electrodes after 20 cycles (scale bar = 10 μm). (d) In-situ Raman characterization of the porous Pt electrode. (e) Gas evolution during cycling of porous Pt electrode.

For further insights into the role of porous-Pt-(111)@CC in enhancing $CO_2$ conversion kinetics and reversibility, in-situ Raman and differential electrochemical mass spectrometry (DEMS) were

conducted to probe the reaction mechanism. As shown in **Figure 3d**, the Raman intensity of reaction product $Li_2CO_3$ (typical peak at ~1090 $cm^{-1}$) and carbon (G-bond at ~1600 $cm^{-1}$ and D-bond at ~1350 $cm^{-1}$) was recorded.[47] During the galvanostatic discharging process, the intensity of the reaction products gradually increased. In the following charging process, the corresponding intensity gradually vanished. This result indicates that apart from $Li_2CO_3$, the evolution of C is also reversible. indicating superior reversibility. DEMS results (**Figure 3e**) show that $CO_2$ was the only gas specie that being consumed/released during discharging/charging. The charge evolution during discharging or charging is $2.93\times10^{-6}$mol (20 μA $cm^{-2}$, 100 μAh $cm^{-2}$). The molar amounts of the consumed and released $CO_2$ based on DEMS are calculated to be $2.192\times10^{-6}$ mol and $2.183\times10^{-6}$ mol for discharging and charging process, respectively. The $CO_2$ mass-to-charge ratio during discharging or charging is very close to 0.75, indicating a highly reversible pathway ($3CO_2+4Li^+\leftrightarrow2Li_2CO_3+C$). Since irreversible Li-$CO_2$ reaction has been reported to generate $O_2$ upon charging process as the following reaction path: $2Li_2CO_3\rightarrow2CO_2+O_2+4Li^++4e^-$,[11, 12] this result has ruled out the above mentioned $Li_2CO_3$ decomposition route and further confirmed the high reversibility of $CO_2$ conversion on porous-Pt-(111)@CC.

**Electrochemical performance under more practical operating conditions**

As previously mentioned, the real application of LCBs relies on their performance under practical current densities. Herein, additional electrochemical tests were carried out to evaluate the battery performance of porous-Pt-(111)@CC. Porous-Pt-(111)@CC exhibited a steady discharging/charging plateau under various current densities (**Figure 4a**) and small overpotentials (**Figure 4b**) of 0.45 V, 0.65 V, 0.89 V and 1.26 V at 20, 40, 80 and 160 μA $cm^{-2}$, respectively, which correspond to energy efficiencies (**Figure 4c**) of 87.5%, 82.1%, 75.6% and 65.9%. In comparison, pristine-Pt@CC exhibited much poorer rate capabilities. The charging voltage of pristine-Pt@CC increased sharply (as high as 4.5 V) with the current density (**Figure S27** and **Figure 4b**), resulting in inferior energy efficiencies of 85.0%, 71.9%, 63.7% and 42.4% at 20, 40, 80 and 160 μA $cm^{-2}$, respectively. To further highlight the excellence of the as-developed porous Pt catalyst, the electrochemical performances (including charging voltage, overpotential and energy efficiency) were compared with previously reported Li-$CO_2$ battery cathode catalysts as summarised in **Figure 4d** and **Table S2**. Porous-Pt-(111)@CC clearly demonstrates the highest energy efficiency and lowest overpotential among all the listed metal or metal-based catalysts even under higher current densities (**Figure S28**). Notably, the as-developed Pt catalyst with optimized catalytic sites also delivered the highest energy efficiency with the minimum areal mass loading compared with previously reported works (**Figure**

S29), indicating a much improved catalyst utilization efficiency.

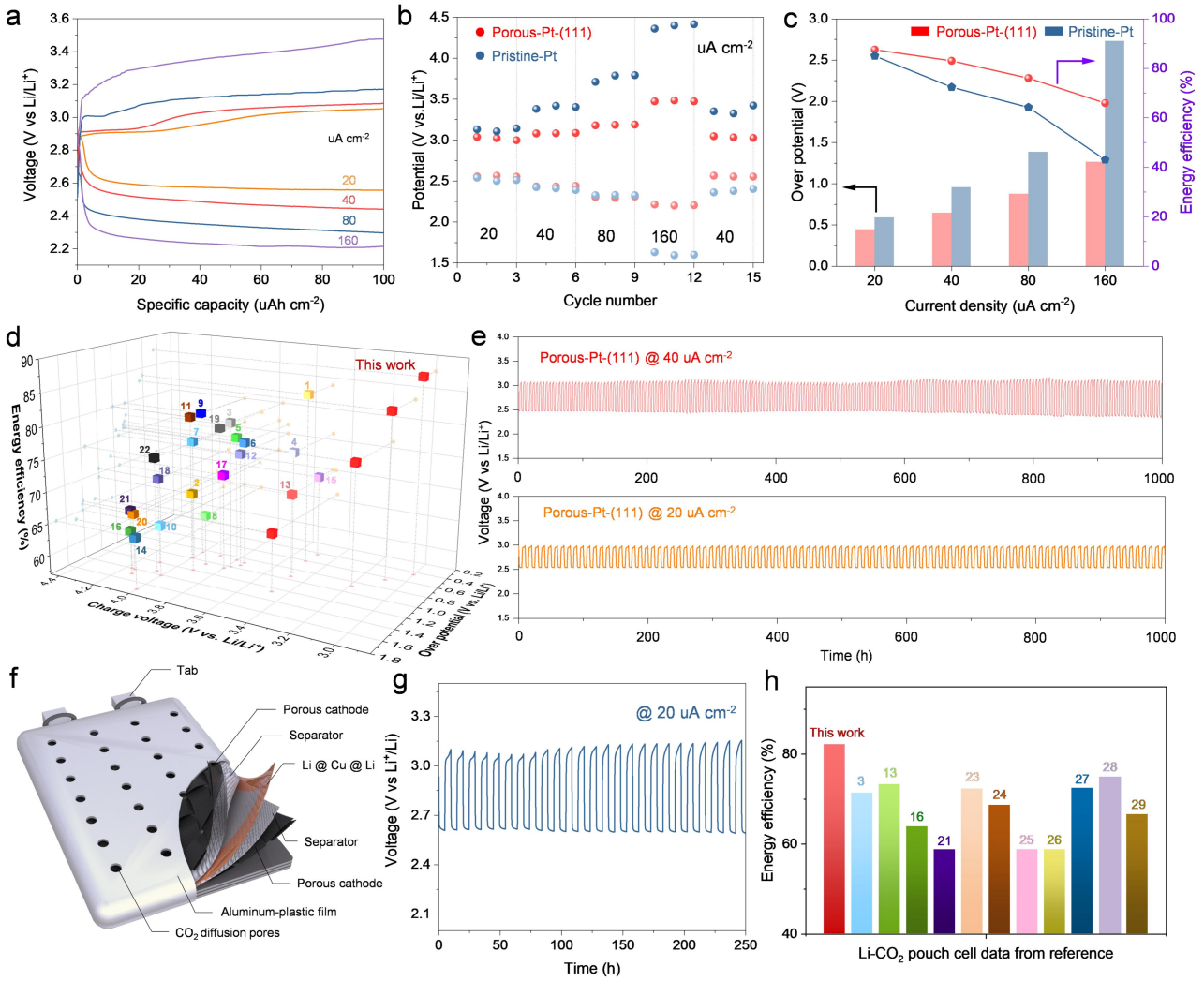


**Figure 4. Electrochemical performance under practical operating conditions.** (a) Voltage-capacity curves under different current densities of porous Pt catalyst, the cut-off capacity of 100 μAh $cm^{-2}$. (b) Charging/discharging voltage under different current densities for different catalysts. (c) Overpotential and energy efficiency under different current densities for different catalysts. (d) Comparison of LCB coin cell performance with literature from **Table S2**. (e) Long cycle performance of porous Pt catalyst-based LCB, under current densities of 20 μA $cm^{-2}$ and 40 μA $cm^{-2}$. (f) Stacked structure of LCB pouch cell. (g) Cycle performance of the stacked LCB pouch cell under 20 μA $cm^{-2}$. (h) Energy efficiency comparison of the Li-$CO_2$ pouch cell performance with literature from **Table S3**.

Owing to the sluggish $CO_2$ conversion kinetics, many reported LCBs are normally cycled at impractically low areal current densities (**Figure S28**). Here, the cycle stability of the LCBs with different electrocatalysts was investigated at the current densities of 20 μA $cm^{-2}$ and 40 μA $cm^{-2}$. As shown in **Figure S30**, pristine-Pt@CC delivered a poor cycle performance under 40 μA $cm^{-2}$. The charging voltage already reached 3.5 V within the first 10 cycles and gradually increased up to 4.5 V during sequential cycles. Worse still, the discharging voltage also dropped below 1.5 V, leading to disastrous energy efficiencies. The pure carbon electrode exhibited even poorer cycle performance as

shown in **Figure S31**. Remarkably, excellent cycle stability was exhibited by porous-Pt-(111)@CC as shown in **Figure 4e**. Under current densities of 20 μA $cm^{-2}$, the as-assembled LCBs can be stably cycled for over 100 cycles (> 1000 hours) with an average low overpotential of 0.5 V. Under the elevated current density of 40 μA $cm^{-2}$, LCBs based on the porous-Pt-(111) catalyst can be cycled over 1000 hours (corresponding to over 200 cycles) with high energy efficiency of over 80% (**Figure S32**), evidencing that the high-rate performance and cycling stability can be simultaneously achieved by porous-Pt-(111)@CC. The porous-Pt-(111) catalyst based LCBs were further operated under higher specific areal capacity (200 μAh $cm^{-2}$). Low overpotential (**Figure S33**) and stable cycle performance (**Figure S34**) remained demonstrating the enhanced $CO_2$ conversion kinetics.

Single-layer Li-$CO_2$ pouch cells have been previously reported, but many of them can only power low-energy or low-power electronics with the limited practical operation.[37, 48-50] Developing practical pouch-cell-level Li-$CO_2$ batteries puts forward a challenging opportunity to realise the potential $CO_2$ utilisation and energy storage ability of Li-$CO_2$ batteries. Here, to further demonstrate the potential of porous-Pt-(111)@CC in practical application scenarios, proof-of-concept stacked Li-$CO_2$ pouch cells (**Figure 4f**) with two layers of air electrodes were assembled and tested. Under the current densities of 20 μA $cm^{-2}$, the stacked Li-$CO_2$ pouch cell delivered a total capacity of 280 $mAh_{cell}$ (**Figure S35**). Apart from lighting the LED arrays as shown in **Figure S36**, the as-developed stacked Li-$CO_2$ pouch cell can be stably cycled under 20 μA $cm^{-2}$ (**Figure 4g**) with low overpotential (0.5 V) and high energy efficiency (82.2%) (**Figure S37**). Compared with the reported Li-$CO_2$ pouch cells (**Figure 4h**, **Figure S38** and **Table S3**), the stable cycling of the porous Pt based stacked Li-$CO_2$ pouch cells with low overpotential and high energy efficiency demonstrates its potential for large scale application. Considering the utilization cost, the Pt/Carbon weight ratio in our cathode electrode is calculated to be 0.77 wt.% which is only one-fourth of that in the commercial Pt/C catalyst (3 wt.%). Meanwhile, no harmful or expensive chemicals are used during the synthesis process. Overall, compared with the traditional wet chemistry routine to synthesis electrocatalyst, the proposed catalyst regulation strategy not only provides a rapid, cost-effective, and controllable approach to enhance the LCBs, but also inspires synthesis of catalysts based on non-noble metals. Furthermore, through the strategy of simultaneously tuning the crystalline facets and morphology, catalysts that previously considered ineffective might be revived.

## Conclusions

In summary, following the theoretical identification of the highly efficient catalytic orientation of platinum catalyst toward $CO_2$ conversion for LCBs, a porous Pt catalyst (porous-Pt-(111)@CC) with

preferred orientation of (111) has been controllably and efficiently developed by fast electrical joule heating techniques. Benefiting from the improved $CO_2$ conversion kinetics on the (111) facet (including compatibility and affinity toward reactant, and the lower energy barrier for $Li_2CO_3$ decomposition), porous-Pt-(111)@CC delivered remarkable electrochemical performance with minimum catalyst loading. Areal capacity could be doubled owing to the porous structure that with abundant catalytic reaction sites to accommodate reaction products. Ex-situ and in-situ characterizations have confirmed the high reversibility of the as-developed porous pt catalyst, which ensures the stable long-term cycling of LCBs with low overpotential and ultrahigh energy efficiency, outperforming most reported metal or metal-based electrocatalysts for LCBs. A proof-of-concept stacked Li-$CO_2$ pouch cells are further fabricated and delivered considerable areal capacity and stable cycle performance under 0.2 C, demonstrating its potential in practical use. The proposed strategy to regulate specific catalytic sites and consequently maximize the utilization of catalysts provides a rational and eco-efficient approach for the synthesis of advanced catalysts toward next-generation high-performance energy conversion and storage devices.

**Acknowledgements**

L. Y. acknowledge the support from Shenzhen Science and Technology Planning Project (JSGG20220831095604008). K.Y and Y.Z. acknowledge support from the EPSRC New Investigator Award (EP/V002260/1) “Scalable fabrication of on-chip Li-$CO_2$ batteries for efficient electrocatalysts screening and energy storage mechanism study” and the Faraday Institute - Battery Study and Seed Research Project “Rational design and manufacture of stacked Li-$CO_2$ pouch cells”.

**Competing interests**

The authors declare no competing interests.

## References


[1] T. Ahmad, S. Liu, M. Sajid, K. Li, M. Ali, L. Liu, W. Chen, Electrochemical $CO_2$ reduction to $C_{2+}$ products using Cu-based electrocatalysts: A review, Nano Research Energy 1 (2022) e9120021. https://doi.org/10.26599/NRE.2022.9120021.

[2] J.-J. Wang, X.-P. Li, B.-F. Cui, Z. Zhang, X.-F. Hu, J. Ding, Y.-D. Deng, X.-P. Han, W.-B. Hu, A review of non-noble metal-based electrocatalysts for $CO_2$ electroreduction, Rare Metals 40(11) (2021) 3019-3037. https://doi.org/10.1007/s12598-021-01736-x.

[3] Z. Xie, X. Zhang, Z. Zhang, Z. Zhou, Metal–$CO_2$ Batteries on the Road: $CO_2$ from Contamination Gas to Energy Source, Advanced Materials 29(15) (2017) 1605891. https://doi.org/10.1002/adma.201605891.

[4] J. Wang, B. Marchetti, X.-D. Zhou, S. Wei, Heterogeneous Electrocatalysts for Metal–$CO_2$ Batteries and CO2 Electrolysis, ACS Energy Letters (2023) 1818-1838. https://doi.org/10.1021/acsenergylett.2c02445.

[5] H. Han, S. Jin, S. Park, Y. Kim, D. Jang, M.H. Seo, W.B. Kim, Plasma-induced oxygen vacancies in amorphous MnOx boost catalytic performance for electrochemical $CO_2$ reduction, Nano Energy 79 (2021) 105492. https://doi.org/10.1016/j.nanoen.2020.105492.

[6] Z. Wang, B. Liu, X. Yang, C. Zhao, P. Dong, X. Li, Y. Zhang, K. Doyle-Davis, X. Zeng, Y. Zhang, X. Sun, Dual Catalytic Sites of Alloying Effect Bloom $CO_2$ Catalytic Conversion for Highly Stable Li–$CO_2$ Battery, Advanced Functional Materials 33(28) (2023) 2213931. https://doi.org/10.1002/adfm.202213931.

[7] J. Choi, S. Park, H. Han, M. Kim, M. Park, J. Han, W.B. Kim, Highly efficient CO2 electrolysis to CO on Ruddlesden–Popper perovskite oxide with in situ exsolved Fe nanoparticles, Journal of Materials Chemistry A 9(13) (2021) 8740-8748. https://doi.org/10.1039/D0TA11328J.

[8] S. Zhang, L. Sun, Q. Fan, F. Zhang, Z. Wang, J. Zou, S. Zhao, J. Mao, Z. Guo, Challenges and prospects of lithium–$CO_2$ batteries, Nano Research Energy 1 (2022) e9120001. https://doi.org/10.26599/NRE.2022.9120001.

[9] W. Huang, J. Qiu, Y. Ji, W. Zhao, Z. Dong, K. Yang, M. Yang, Q. Chen, M. Zhang, C. Lin, K. Xu, L. Yang, F. Pan, Exploiting Cation Intercalating Chemistry to Catalyze Conversion-Type Reactions in Batteries, ACS Nano 17(6) (2023) 5570-5578. https://doi.org/10.1021/acsnano.2c11029.

[10] Y. Liu, R. Mao, B. Chen, B. Lu, Z. Piao, Y. Song, G. Zhou, H.-M. Cheng, Atomic design of bidirectional electrocatalysts for reversible Li-$CO_2$ batteries, Materials Today (2023). https://doi.org/10.1016/j.mattod.2022.12.008.

[11] J. Lin, W. Song, C. Xiao, J. Ding, Z. Huang, C. Zhong, J. Ding, W. Hu, A comprehensive overview of the electrochemical mechanisms in emerging alkali metal–carbon dioxide batteries, Carbon Energy (2023). https://doi.org/10.1002/cey2.313.

[12] Y. Jiao, J. Qin, H.M.K. Sari, D. Li, X. Li, X. Sun, Recent progress and prospects of Li-$CO_2$ batteries: Mechanisms, catalysts and electrolytes, Energy Storage Materials 34 (2021) 148-170. https://doi.org/10.1016/j.ensm.2020.09.014.

[13] J. Li, A. Dai, K. Amine, J. Lu, Correlating Catalyst Design and Discharged Product to Reduce

Overpotential in Li-$CO_2$ Batteries, Small 17(48) (2021) 2007760. https://doi.org/10.1002/smll.202007760.
[14] X. Mu, H. Pan, P. He, H. Zhou, Li–$CO_2$ and Na–$CO_2$ Batteries: Toward Greener and Sustainable Electrical Energy Storage, 32(27) (2020) 1903790. https://doi.org/10.1002/adma.201903790.
[15] Y. Xu, H. Gong, L. Song, Y. Kong, C. Jiang, H. Xue, P. Li, X. Huang, J. He, T. Wang, A highly efficient and free-standing copper single atoms anchored nitrogen-doped carbon nanofiber cathode toward reliable Li–$CO_2$ batteries, Materials Today Energy 25 (2022) 100967. https://doi.org/10.1016/j.mtener.2022.100967.
[16] J. Lin, J. Ding, H. Wang, X. Yang, X. Zheng, Z. Huang, W. Song, J. Ding, X. Han, W. Hu, Boosting Energy Efficiency and Stability of Li–CO2 Batteries via Synergy between Ru Atom Clusters and Single-Atom Ru–N4 sites in the Electrocatalyst Cathode, Advanced Materials 34(17) (2022) 2200559. https://doi.org/10.1002/adma.202200559.
[17] R. Li, J. Xu, Q. Zhao, W. Ren, R. Zeng, Q. Pan, X. Yan, J. Ba, T. Tang, W. Luo, Cathodic corrosion as a facile and universal method for the preparation of supported metal single atoms, Nano Research 15(3) (2022) 1838-1844. https://doi.org/10.1007/s12274-021-3767-3.
[18] C.D. Koolen, W. Luo, A. Züttel, From Single Crystal to Single Atom Catalysts: Structural Factors Influencing the Performance of Metal Catalysts for $CO_2$ Electroreduction, ACS Catalysis 13(2) (2023) 948-973. https://doi.org/10.1021/acscatal.2c03842.
[19] F. Lü, H. Bao, Y. Mi, Y. Liu, J. Sun, X. Peng, Y. Qiu, L. Zhuo, X. Liu, J. Luo, Electrochemical $CO_2$ reduction: from nanoclusters to single atom catalysts, Sustainable Energy & Fuels 4(3) (2020) 1012-1028. https://doi.org/10.1039/C9SE00776H.
[20] G. Giannakakis, M. Flytzani-Stephanopoulos, E.C.H. Sykes, Single-Atom Alloys as a Reductionist Approach to the Rational Design of Heterogeneous Catalysts, Accounts of Chemical Research 52(1) (2019) 237-247. https://doi.org/10.1021/acs.accounts.8b00490.
[21] Z. Chen, J. Liu, M.J. Koh, K.P. Loh, Single-Atom Catalysis: From Simple Reactions to the Synthesis of Complex Molecules, Advanced Materials 34(25) (2022) 2103882. https://doi.org/10.1002/adma.202103882.
[22] A.K. Chourasia, A.D. Pathak, C. Bongu, K. Manikandan, S. Praneeth, K.M. Naik, C.S. Sharma, In Situ/Operando Characterization Techniques: The Guiding Tool for the Development of Li–$CO_2$ Battery, Small Methodes 6(12) (2022) 2200930. https://doi.org/10.1002/smtd.202200930.
[23] B. Lu, B. Chen, D. Wang, C. Li, R. Gao, Y. Liu, R. Mao, J. Yang, G. Zhou, Engineering the interfacial orientation of $MoS_2/Co_9S_8$ bidirectional catalysts with highly exposed active sites for reversible Li-$CO_2$ batteries, Proceedings of the National Academy of Sciences of the United States of America 120(6) (2023) e2216933120. https://doi.org/doi:10.1073/pnas.2216933120.
[24] B. Chen, D. Wang, B. Zhang, X. Zhong, Y. Liu, J. Sheng, Q. Zhang, X. Zou, G. Zhou, H.-M. Cheng, Engineering the Active Sites of Graphene Catalyst: From $CO_2$ Activation to Activate Li-CO2 Batteries, ACS Nano 15(6) (2021) 9841-9850. https://doi.org/10.1021/acsnano.1c00756.
[25] B. Chen, D. Wang, J. Tan, Y. Liu, M. Jiao, B. Liu, N. Zhao, X. Zou, G. Zhou, H.-M. Cheng, Designing Electrophilic and Nucleophilic Dual Centers in the $ReS_2$ Plane toward Efficient Bifunctional Catalysts for Li-$CO_2$ Batteries, Journal of the American Chemical Society 144(7) (2022) 3106-3116.

https://doi.org/10.1021/jacs.1c12096.

[26] Y. Yao, Z. Huang, P. Xie, S.D. Lacey, R.J. Jacob, H. Xie, F. Chen, A. Nie, T. Pu, M. Rehwoldt, D. Yu, M.R. Zachariah, C. Wang, R. Shahbazian-Yassar, J. Li, L. Hu, Carbothermal shock synthesis of high-entropy-alloy nanoparticles, Science 359(6383) (2018) 1489-1494. https://doi.org/10.1126/science.aan5412.

[27] S. Xu, G. Zhong, C. Chen, M. Zhou, D.J. Kline, R.J. Jacob, H. Xie, S. He, Z. Huang, J. Dai, A.H. Brozena, R. Shahbazian-Yassar, M.R. Zachariah, S.M. Anlage, L. Hu, Uniform, Scalable, High-Temperature Microwave Shock for Nanoparticle Synthesis through Defect Engineering, Matter 1(3) (2019) 759-769. https://doi.org/10.1016/j.matt.2019.05.022.

[28] Y. Jin, C. Hu, Q. Dai, Y. Xiao, Y. Lin, J.W. Connell, F. Chen, L. Dai, High-Performance Li-$CO_2$ Batteries Based on Metal-Free Carbon Quantum Dot/Holey Graphene Composite Catalysts, Advanced Functional Materials 28(47) (2018) 1804630. https://doi.org/10.1002/adfm.201804630.

[29] S. Liu, Y. Shen, Y. Zhang, B. Cui, S. Xi, J. Zhang, L. Xu, S. Zhu, Y. Chen, Y. Deng, W. Hu, Extreme Environmental Thermal Shock Induced Dislocation-Rich Pt Nanoparticles Boosting Hydrogen Evolution Reaction, Advanced Materials 34(2) (2022) 2106973. https://doi.org/10.1002/adma.202106973.

[30] M.K. Carpenter, T.E. Moylan, R.S. Kukreja, M.H. Atwan, M.M. Tessema, Solvothermal Synthesis of Platinum Alloy Nanoparticles for Oxygen Reduction Electrocatalysis, Journal of the American Chemical Society 134(20) (2012) 8535-8542. https://doi.org/10.1021/ja300756y.

[31] S.M. Geyer, R. Methaapanon, R. Johnson, S. Brennan, M.F. Toney, B. Clemens, S. Bent, Structural evolution of platinum thin films grown by atomic layer deposition, Journal of Applied Physics 116(6) (2014) 064905. https://doi.org/10.1063/1.4892104.

[32] J. Zhu, D. Xiao, W. Peng, F. Lan, D. Wan, Influence of Rapid Thermal Processing on the Orientation Properties of $PbTiO_3$ Thin Film, Crystal Research and Technology 32(3) (1997) 449-453. https://doi.org/10.1002/crat.2170320312.

[33] W. Wang, Z. Wang, M. Yang, C.-J. Zhong, C.-J. Liu, Highly active and stable Pt (111) catalysts synthesized by peptide assisted room temperature electron reduction for oxygen reduction reaction, Nano Energy 25 (2016) 26-33. https://doi.org/10.1016/j.nanoen.2016.04.022.

[34] M. Wang, H. Liu, J. Ma, G. Lu, The activity enhancement of photocatalytic water splitting by F- pre-occupation on Pt(100) and Pt(111) co-catalyst facets, Applied Catalysis B: Environmental 266 (2020) 118647. https://doi.org/10.1016/j.apcatb.2020.118647.

[35] C. Li, N. Clament Sagaya Selvam, J. Fang, Shape-Controlled Synthesis of Platinum-Based Nanocrystals and Their Electrocatalytic Applications in Fuel Cells, Nano-Micro Letters 15(1) (2023) 83. https://doi.org/10.1007/s40820-023-01060-2.

[36] K. Wang, D. Liu, L. Liu, X. Li, H. Wu, Z. Sun, M. Li, A.S. Vasenko, S. Ding, F. Wang, C. Xiao, Isolated Metalloid Tellurium Atomic Cluster on Nitrogen-Doped Carbon Nanosheet for High-Capacity Rechargeable Lithium-$CO_2$ Battery, Advanced Science 10(7) (2023) 2205959. https://doi.org/10.1002/advs.202205959.

[37] Q. Deng, Y. Yang, C. Mao, T. Wang, Z. Fang, W. Yan, K. Yin, Y. Zhang, Electronic State Modulation and Reaction Pathway Regulation on Necklace-Like $MnO_x$-$CeO_2$@Polypyrrole Hierarchical Cathode for

Advanced and Flexible Li–$CO_2$ Batteries, Advanced Energy Materials 12(14) (2022) 2103667. https://doi.org/10.1002/aenm.202103667.

[38] J. Zhou, T. Wang, L. Chen, L. Liao, Y. Wang, S. Xi, B. Chen, T. Lin, Q. Zhang, C. Ye, X. Zhou, Z. Guan, L. Zhai, Z. He, G. Wang, J. Wang, J. Yu, Y. Ma, P. Lu, Y. Xiong, S. Lu, Y. Chen, B. Wang, C.-S. Lee, J. Cheng, L. Gu, T. Zhao, Z. Fan, Boosting the reaction kinetics in aprotic lithium-carbon dioxide batteries with unconventional phase metal nanomaterials, Proceedings of the National Academy of Sciences of the United States of America 119(40) (2022) e2204666119. https://doi.org/doi:10.1073/pnas.2204666119.

[39] L. Chen, J. Zhou, J. Zhang, G. Qi, B. Wang, J. Cheng, Copper Indium Sulfide Enables Li-$CO_2$ Batteries with Boosted Reaction Kinetics and Cycling Stability, Energy & Environmental Materials 0 (2022) 1. https://doi.org/10.1002/eem2.12415.

[40] P.-F. Zhang, T. Sheng, Y. Zhou, Y.-J. Wu, C.-C. Xiang, J.-X. Lin, Y.-Y. Li, J.-T. Li, L. Huang, S.-G. Sun, Li-$CO_2$/$O_2$ battery operating at ultra-low overpotential and low $O_2$ content on Pt/CNT catalyst, Chemical Engineering Journal 448 (2022) 137541. https://doi.org/10.1016/j.cej.2022.137541.

[41] Y. Jin, F. Chen, J. Wang, Achieving Low Charge Overpotential in a Li-$CO_2$ Battery with Bimetallic RuCo Nanoalloy Decorated Carbon Nanofiber Cathodes, ACS Sustainable Chemistry & Engineering 8(7) (2020) 2783-2792. https://doi.org/10.1021/acssuschemeng.9b06668.

[42] Y. Qiao, J. Yi, S. Wu, Y. Liu, S. Yang, P. He, H. Zhou, Li-$CO_2$ Electrochemistry: A New Strategy for $CO_2$ Fixation and Energy Storage, Joule 1(2) (2017) 359-370. https://doi.org/10.1016/j.joule.2017.07.001.

[43] X. Zhang, T. Wang, Y. Yang, X. Zhang, Z. Lu, J. Wang, C. Sun, Y. Diao, X. Wang, J. Yao, Breaking the Stable Triangle of Carbonate via W–O Bonds for Li-$CO_2$ Batteries with Low Polarization, ACS Energy Letters 6(10) (2021) 3503-3510. https://doi.org/10.1021/acsenergylett.1c01428.

[44] Z.-Z. Shen, Y.-Z. Zhang, C. Zhou, R. Wen, L.-J. Wan, Revealing the Correlations between Morphological Evolution and Surface Reactivity of Catalytic Cathodes in Lithium–Oxygen Batteries, Journal of the American Chemical Society 143(51) (2021) 21604-21612. https://doi.org/10.1021/jacs.1c09700.

[45] O. Keisar, Y. Ein-Eli, Y. Alfi, Y. Cohen, Insights into the surface and stress behavior of manganese-oxide catalyst during oxygen reduction reaction, Journal of Power Sources 450 (2020) 227545. https://doi.org/10.1016/j.jpowsour.2019.227545.

[46] H. Dykes, Rosy, D. Sharon, M. Noked, Ö. Çapraz, In Situ Stress Measurements on Thin Film Au Positive Electrode during the First Discharge of Li-$O_2$ Batteries, Journal of The Electrochemical Society 168(11) (2021) 110551. https://doi.org/10.1149/1945-7111/ac3937.

[47] T. Jian, W. Ma, C. Xu, H. Liu, J. Wang, Intermetallic-driven highly reversible electrocatalysis in Li–$CO_2$ battery over nanoporous $Ni_3Al$/Ni heterostructure, eScience (2023) 100114. https://doi.org/10.1016/j.esci.2023.100114.

[48] G. Qi, J. Zhang, L. Chen, B. Wang, J. Cheng, Binder-Free MoN Nanofibers Catalysts for Flexible 2-Electron Oxalate-Based Li-$CO_2$ Batteries with High Energy Efficiency, Advanced Functional Materials 32(22) (2022) 2112501. https://doi.org/10.1002/adfm.202112501.

[49] Y. Wang, J. Zhou, C. Lin, B. Chen, Z. Guan, A.M. Ebrahim, G. Qian, C. Ye, L. Chen, Y. Ge, Q. Yun, X.

Wang, X. Zhou, G. Wang, K. Li, P. Lu, Y. Ma, Y. Xiong, T. Wang, L. Zheng, S. Chu, Y. Chen, B. Wang, C.-S. Lee, Y. Liu, Q. Zhang, Z. Fan, Decreasing the Overpotential of Aprotic Li-$CO_2$ Batteries with the In-Plane Alloy Structure in Ultrathin 2D Ru-Based Nanosheets, Advanced Functional Materials 32(30) (2022) 2202737. https://doi.org/10.1002/adfm.202202737.

[50] L. Liu, Y. Qin, K. Wang, H. Mao, H. Wu, W. Yu, D. Zhang, H. Zhao, H. Wang, J. Wang, C. Xiao, Y. Su, S. Ding, Rational Design of Nanostructured Metal/C Interface in 3D Self-Supporting Cellulose Carbon Aerogel Facilitating High-Performance Li-$CO_2$ Batteries, Advanced Energy Materials 12(20) (2022) 2103681. https://doi.org/10.1002/aenm.202103681.